Capacity for Noncoherent, Soft-Decision MFSK Signaling

S. Butman and B. K. Levitt
Communications Systems Research Section

Planetary probes into the dense atmospheres of Venus, Jupiter, and Saturn may require noncoherent communication links to Earth. In this article, the capacity of noncoherent, multiple-frequency shift-keyed (MFSK) systems is determined as a function of the number of frequencies, receiver quantization, and signal-to-noise ratio. It is shown that the spacing of the quantizer levels is not critical, and that 8-level uniform quantization is essentially as good as infinite quantization.

I. Introduction

Entry probes into the turbulent and dispersive atmospheres of Venus, Jupiter, and Saturn may require noncoherent, multiple-frequency shift-keyed (MFSK) communication systems as direct or relay links to Earth. Bar-David and Butman (Ref. 1) have computed the capacity and the convolutional coding rate parameter R_{comp} (Ref. 2) for such channels with hard-decision receivers. Choudhury (Ref. 3) has evaluated the parameters R_{comp} and $E_0(\rho)$ (Ref. 4) for noncoherent MFSK systems with quantized (soft-decision) receivers. In this article, the channel capacity is determined for soft-decision receivers as a function of the number of frequencies, the predetection signal-to-noise ratio, and the number of uniformly spaced quantization levels, after the spacing of these levels has been optimized. The results are compared to the channel capacity of an unquantized MFSK receiver, which has been computed for binary and infinite signal sets.

In order to minimize the cost of providing a given link capability, it is important to know the capacity of a channel before design decisions are made. This information is also relevant to flight/ground tradeoffs involving relay versus direct links, relay link versus downlink complexity, and ground versus probe/relay bus complexity.

II. Infinite Quantization Capacity

Consider a set of M equally likely orthogonal signals $\{s_i;\ 1 \leq i \leq M\}$ transmitted over an additive white Gaussian noise (AWGN) channel. (Once we are restricted to

orthogonal signals, it is reasonable to use this channel model.) For each transmission, a noncoherent square-law receiver generates a vector observable $\mathbf{r} = (r_1, r_2, \cdots, r_M)$ with continuous, independent components which are the outputs of the M envelope detectors. Using symmetry, it is well known (Ref. 4) that the channel capacity $C_M(\alpha)$ is given by

$$C_M(\alpha) = \frac{1}{T}\int_{\mathbf{r}} d\mathbf{r}\, p(\mathbf{r} \mid s_1) \log_2\left[\frac{p(\mathbf{r} \mid s_1)}{p(\mathbf{r})}\right] \text{bits/second} \quad (1)$$

where T is the signal duration in seconds, $p(\mathbf{r} \mid s_1)$ is the conditional density of $\mathbf{r}$ given that s_1 is sent, and $p(\mathbf{r})$ is the density of $\mathbf{r}$. It can be shown (Ref. 5) that the conditional density of the jth envelope detector output r_j has the form

$$p(r_j \mid s_i) = \begin{cases} r_i \exp\left[-\frac{1}{2}(r_i^2 + \alpha^2)\right] I_0(\alpha r_i); & j = i \\ r_j \exp\left[-\frac{r_j^2}{2}\right]; & j \neq i \end{cases} \quad (2)$$

where

$$\frac{\alpha^2}{2} = \frac{ST}{N_0} \quad (3)$$

is the signal-to-noise ratio in the predetection filter. Consequently, Eq. (1) can be expressed as

$$\frac{C_M(\alpha)}{C_\infty} = \frac{2}{\alpha^2}\exp\left[-\frac{\alpha^2}{2}\right]\int_{\mathbf{r}} d\mathbf{r}\, I_0(\alpha r_1) \times \prod_{j=1}^{M} r_j \exp\left[-\frac{r_j^2}{2}\right] \ln\left[\frac{I_0(\alpha r_1)}{\frac{1}{M}\sum_{i=1}^{M} I_0(\alpha r_i)}\right] \quad (4)$$

where

$$C_\infty = \left(\frac{S}{N_0}\right)\log_2 e \text{ bits/second} \quad (5)$$

is the familiar expression (Ref. 2) for the capacity of the infinite-bandwidth, coherent AWGN channel.

In general, the multiple integral in Eq. (4) cannot be evaluated in closed form. However, it has been shown (Ref. 6) that $C_M(\alpha)/C_\infty$ increases monotonically with increasing M to the limiting value

$$\frac{C_\infty(\alpha)}{C_\infty} = \frac{2}{\alpha^2}\exp\left[-\frac{\alpha^2}{2}\right] \times \int_0^\infty dx\, x \exp\left[-\frac{x^2}{2}\right] I_0(\alpha x) \ln I_0(\alpha x) - 1 \quad (6)$$

which can be calculated numerically, and is plotted together with the soft-decision capacity curves as the ultimate performance limit for noncoherent MFSK systems. Equation (6) also compares the infinite-bandwidth capacities for coherent and noncoherent signaling over an AWGN channel as a function of the received signal-to-noise ratio $\alpha^2/2$. Also of interest is the binary signaling case, for which Eq. (4) reduces to a double integral which can be computed numerically:

$$\frac{C_2(\alpha)}{C_\infty} = \frac{2}{\alpha^2}\exp\left[-\frac{\alpha^2}{2}\right]\int_0^\infty dx\, x \exp\left[-\frac{x^2}{2}\right] I_0(\alpha x) \times \int_0^\infty dy\, y \exp\left[-\frac{y^2}{2}\right] \ln\left[\frac{2I_0(\alpha x)}{I_0(\alpha x) + I_0(\alpha y)}\right] \quad (7)$$

Equation (7) is the limiting capacity for binary, noncoherent MFSK signaling with a soft-decision receiver (see Figs. 2 and 6).

III. Soft-Decision Capacity

A. Binary Single-Observable Case

Consider a special case of binary noncoherent frequency shift-keyed (FSK) signaling in which the sufficient observable

$$r = r_1^2 - r_2^2 \quad (8)$$

is formed from the envelope detector outputs r_1 and r_2: this will hereafter be referred to as the single-observable (SO) case. A soft-decision receiver forms the discrete observable q by quantizing the continuous observable r to one of Q levels. For simplicity, a uniform quantization scheme with intervals of width Δ is used, as shown in Fig. 1. For this quantization rule, the conditional probability of q satisfies the constraint

$$P(q \mid s_2) = P(Q + 1 - q \mid s_1) \quad (9)$$

Consequently, the normalized capacity can be expressed in the form

$$\frac{C_{SO}(\alpha, Q)}{C_\infty} = \frac{2}{\alpha^2}\sum_{q=1}^{Q} P(q \mid s_1) \ln\left[\frac{2P(q \mid s_1)}{P(q \mid s_1) + P(Q + 1 - q \mid s_1)}\right] \quad (10)$$

It remains to determine the conditional probability $P(q \mid s_1)$, which can be written in terms of the conditional cumulative distribution function

$$F_r(\beta \mid s_1) \equiv P(-\infty < r \leq \beta \mid s_1):$$

$$P(q \mid s_1) = \begin{cases} F_r\left[\Delta\left(1 - \frac{Q}{2}\right) \middle| s_1\right]; & q = 1 \\ F_r\left[\Delta\left(q - \frac{Q}{2}\right) \middle| s_1\right] - F_r\left[\Delta\left(q - \frac{Q}{2} - 1\right) \middle| s_1\right]; & 2 \leq q \leq Q-1 \\ 1 - F_r\left[\Delta\left(\frac{Q}{2} - 1\right) \middle| s_1\right]; & q = Q \end{cases} \tag{11}$$

After some mathematical manipulation, it is found that

$$F_r(\beta \mid s_1) = \begin{cases} \frac{1}{2}\exp\left[\frac{\beta}{2} - \frac{\alpha^2}{4}\right]; & \beta \leq 0 \\ \frac{1}{2}\exp\left[\frac{\beta}{2} - \frac{\alpha^2}{4}\right] Q_M\left(\frac{\alpha}{\sqrt{2}}, \sqrt{2\beta}\right) & \\ \quad + 1 - Q_M(\alpha, \sqrt{\beta}); & \beta \geq 0 \end{cases} \tag{12}$$

where $Q_M(\cdot\ ,\ \cdot)$ is the Marcum Q function (Ref. 7), defined by

$$Q_M(a, b) \equiv \int_b^\infty dx\, x \exp\left[-\frac{1}{2}(x^2 + a^2)\right] I_0(ax) \tag{13}$$

which can be evaluated numerically.

For the special case where $Q = 2$, the binary single-observable system above reduces to the binary, noncoherent MFSK channel with a hard-decision receiver. The normalized capacity in Eq. (10) simplifies to the form

$$\frac{C_{SO}(\alpha, 2)}{C_\infty} = \frac{2}{\alpha^2}[\ln 2 + \varepsilon \ln \varepsilon + (1 - \varepsilon)\ln(1 - \varepsilon)] \tag{14}$$

for a binary symmetric channel with crossover probability

$$\varepsilon = P(1 \mid s_1) = \frac{1}{2}\exp\left[-\frac{\alpha^2}{4}\right] \tag{15}$$

Of course, for $Q = 2$, the capacity is independent of the uniform quantizer spacing Δ. For $Q > 2$, the optimum quantization width Δ_{opt} is determined by maximizing $C_{SO}(\alpha, Q)/C_\infty$ over Δ, for the given Q and α. The optimum normalized capacity $C_{SO}(\alpha, Q)/C_\infty$, evaluated at $\Delta = \Delta_{opt}$, is plotted in Fig. 2 as a function of the predetection signal-to-noise ratio $\alpha^2/2$, for several values of Q. Corresponding curves of Δ_{opt} are presented in Fig. 3. The variation in the normalized capacity with Δ is examined in Fig. 4 for $Q = 4$, $\alpha^2/2 = 1$. Conclusions drawn from these graphs are discussed later.

B. General *M*-ary Case

For the general M-ary noncoherent MFSK system, a soft-decision receiver quantizes each envelope detector output r_i into a discrete observable q_i: this defines a vector observable $\mathbf{q} \equiv (q_1, q_2, \cdots, q_M)$, with statistically independent components. Again, Q uniformly spaced quantization levels are used, with separation Δ, as shown in Fig. 5. Then the normalized capacity can be expressed in terms of the conditional probability of $\mathbf{q}$:

$$\frac{C_M(\alpha, Q)}{C_\infty} = \frac{2}{\alpha^2}\sum_{\mathbf{q}} P(\mathbf{q} \mid s_1)\ln\left[\frac{P(\mathbf{q} \mid s_1)}{\frac{1}{M}\sum_{i=1}^{M} P(\mathbf{q} \mid s_i)}\right] \tag{16}$$

For convenience, define the discrete parameters $x(\cdot)$ and $y(\cdot)$ according to

$$P(q_j \mid s_i) = \begin{cases} x(q_i); & j = i \\ y(q_j); & j \neq i \end{cases} \tag{17}$$

Using Eq. (2) in conjunction with the quantization rule of Fig. 5, it can be shown that

$$x(q_i) = \begin{cases} Q_M[\alpha, \Delta(q_i - 1)] - Q_M[\alpha, \Delta q_i]; & \\ \qquad 1 \leq q_i \leq Q - 1 & \\ Q_M[\alpha, \Delta(Q - 1)]; \quad q_i = Q & \end{cases} \tag{18}$$

and

$$y(q_j) = \begin{cases} \exp\left[-\frac{1}{2}\Delta^2(q_j - 1)^2\right] - \exp\left[-\frac{1}{2}\Delta^2 q_j^2\right]; & \\ \qquad 1 \leq q_j \leq Q - 1 & \\ \exp\left[-\frac{1}{2}\Delta^2(Q - 1)^2\right]; \quad q_i = Q & \end{cases} \tag{19}$$

Then Eq. (16) reduces to

$$\frac{C_M(\alpha, Q)}{C_\infty} = \frac{2}{\alpha^2}\left\{\ln M - \sum_{q_1=1}^{Q} x(q_1)\left[\sum_{\mathbf{q}'} f(\mathbf{q}) - \ln z(q_1)\right]\right\}$$

where

$$\mathbf{q}' \equiv (q_2, q_3, \cdots, q_M)$$

$$f(\mathbf{q}) \equiv \prod_{i=2}^{M} y(q_i) \ln \sum_{j=1}^{M} z(q_j) \tag{20}$$

$$z(q_j) \equiv \frac{x(q_j)}{y(q_j)}$$

Again, the normalized capacity $C_M(\alpha, Q)/C_\infty$ should be maximized over the quantization width Δ, thus defining the optimum spacing Δ_{opt} for the given M, Q, and α. Plots of the optimum normalized capacity and Δ_{opt} are presented in Figs. 6 through 12.

For larger values of M, there is a computational problem inherent in Eq. (20). The difficulty lies in the summation of $f(\mathbf{q})$ over the Q^{M-1} distinct vectors $\mathbf{q}'$ for each value of q_1 : even for $Q = 2$, this becomes unwieldy for $M \gtrsim 16$. This problem is partially alleviated in the Appendix.

IV. Results

In this article, expressions were given for the capacity of an M-ary noncoherent MFSK system with a soft-decision receiver. Results for the binary single-observable case are summarized in Figs. 2–4. In Fig. 2, the optimum normalized capacity C_{SO}/C_∞, evaluated at the optimum uniform quantizer spacing Δ_{opt}, is plotted versus the predetection signal-to-noise ratio ST/N_0, for several levels of quantization Q. As Q increases, C_{SO}/C_∞ converges uniformly to the limiting expression in Eq. (7). For practical purposes, it is evident that very little improvement is realized by using more than 8 levels of quantization. For a given value of Q, Fig. 3 demonstrates that Δ_{opt} varies slowly with ST/N_0, particularly for lower values of ST/N_0. Also, it appears that Δ_{opt} is approximately inversely proportional to Q for any given ST/N_0. For fixed values of Q and ST/N_0, C_{SO}/C_∞ has a broad maximum over Δ at Δ_{opt}. For example, for $Q = 4$ and $ST/N_0 = 1$, Fig. 4 shows that C_{SO}/C_∞ has a maximum value of 0.109 at $\Delta = \Delta_{opt} = 3.1$; however, at $\Delta = 2$ and 4, $C_{SO}/C_\infty = 0.107$ and 0.108, respectively.

Results for the general M-ary case are presented in Figs. 6–12. Although it is not illustrated graphically, it is again true that the normalized capacity C_M/C_∞ varies slowly with Δ near Δ_{opt}, for any given M, Q, and ST/N_0, so that the quantizer spacing is not a critical system parameter. Figures 10 and 11 demonstrate that Δ_{opt}

(1) Is approximately constant for small ST/N_0.

(2) Grows slowly with increasing ST/N_0.

(3) Is roughly inversely proportional to Q.

(4) Is relatively insensitive to changes in M for a given Q.

For the binary dual-observable case, Fig. 6 shows that the optimum normalized capacity C_M/C_∞ again converges uniformly to the limiting curve of Eq. (7), as in the single-observable case. A direct comparison of the $M = 2$ curves in Figs. 2 and 6 reveals that the two binary receivers achieve essentially the same capacity for $Q \geqq 4$, and for $Q = 2$ when $ST/N_0 \gtrsim 3$. However, for $Q = 2$ in the range $ST/N_0 \lesssim 3$, the dual-observable system outperforms the single-observable receiver (recall that for $Q = 2$, the single-observable receiver is simply the binary hard-decision receiver). This performance advantage is not without cost: the dual-observable receiver must store 2 bits of information for each transmission when $Q = 2$, compared to 1 bit in the single-observable case (this additional storage requirement may not be important at low rates).

Figures 6–9 demonstrate the rate of convergence of the optimum C_M/C_∞ to limiting expression in Eq. (6) for infinite M and Q. For fixed Q, this convergence appears to be uniform in M. It is evident that for larger values of M, increasing M only produces significant increases in capacity for larger signal-to-noise levels.

Figure 12 demonstrates some interesting receiver tradeoffs. Denote the M-ary soft-decision receiver with Q levels of quantization by (M, Q). The (M, Q) receiver must store $M \log_2 Q$ bits of information for each transmission (this does not apply to the binary single-observable case). An obvious question is: For a given receiver complexity $M \log_2 Q$, which choice of (M, Q) is optimum with regard to maximizing capacity? The answer, not surprisingly, depends on the predetection signal-to-noise level ST/N_0. For example, when $M \log_2 Q = 8$ bits/transmission with $ST/N_0 \lesssim 1.8$, the (4, 4) receiver outperforms the (8, 2) receiver. And for $M \log_2 Q = 16$ bits/transmission, the (8, 4) receiver achieves a higher capacity than the (16, 2) receiver over the range $ST/N_0 \lesssim 3.9$.

Generalizing these results, it appears that for lower values of ST/N_0, with a given receiver complexity $M \log_2 Q$, it is better to use fewer signals and increase the number of quantization levels. Figure 12 also demonstrates that the (4, 4) receiver has a slightly higher capacity than the (16, 2) receiver over the range $ST/N_0 \lesssim 0.6$, and yet the storage requirements of the former are only half those of the latter.

Acknowledgment

The authors are indebted to I. Eisenberger for numerically computing the integral expressions in Eqs. (6) and (7).

References

1. Bar-David, I., and Butman, S., "Performance of Coded, Noncoherent, Hard-Decision MFSK Systems," in *The Deep Space Network Progress Report*, Technical Report 32-1526, Vol. XIII, pp. 82–91. Jet Propulsion Laboratory, Pasadena, Calif., Feb. 15, 1973.
2. Wozencraft, J. M., and Jacobs, I. M., *Principles of Communications Engineering*, John Wiley & Sons, Inc., New York, 1965.
3. Choudhury, A. K., *Performance of Convolution Coding Concatenated with MFSK Modulation in a Gaussian Channel*, Goddard Space Flight Center, Greenbelt, Md., Dec. 1971.
4. Gallager, R. G., *Information Theory and Reliable Communication*, John Wiley & Sons, Inc., New York, 1968.
5. Viterbi, A. J., *Principles of Coherent Communication*, McGraw-Hill Book Co., Inc., New York, 1966.
6. Butman, S., and Klass, M., "Wideband MFSK System Capacity," to be published in *The Deep Space Network Progress Report*, Technical Report 32-1526, Jet Propulsion Laboratory, Pasadena, Calif.
7. Marcum, J. I., "A Statistical Theory of Target Detection by Pulsed Radar," *IRE Trans. Information Theory*, Vol. IT-6, pp. 159–160, Apr. 1960.

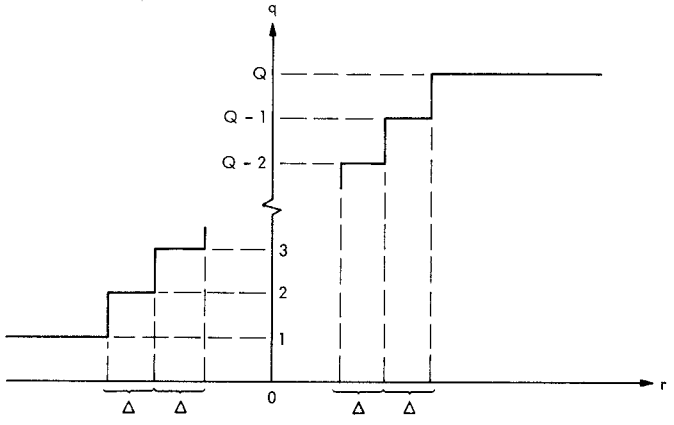

Fig. 1. Quantization rule for binary single-observable case

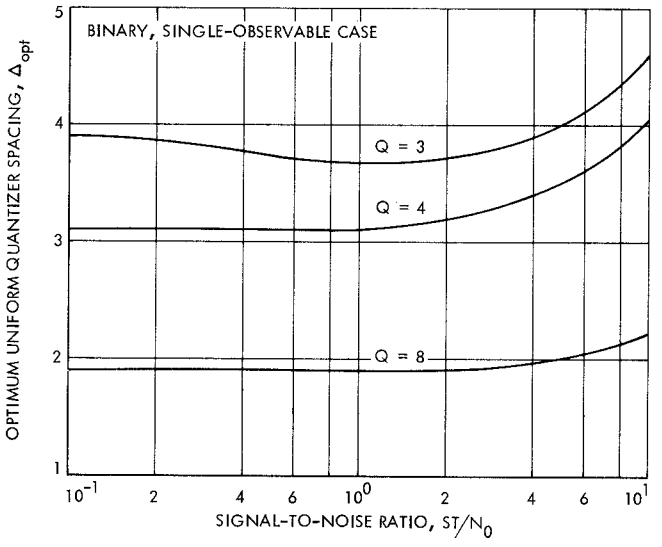

Fig. 3. Optimum quantizer spacing for binary single-observable case

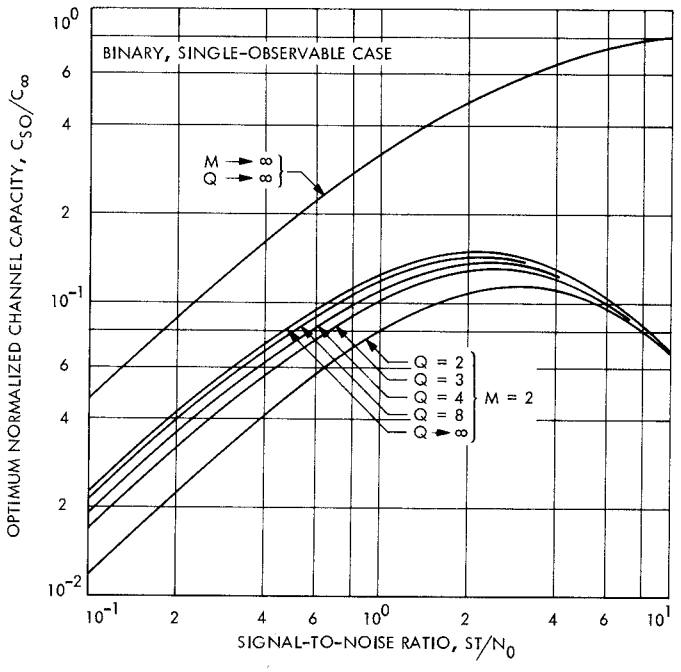

Fig. 2. Capacity for binary noncoherent FSK system based on uniformly quantized single observable

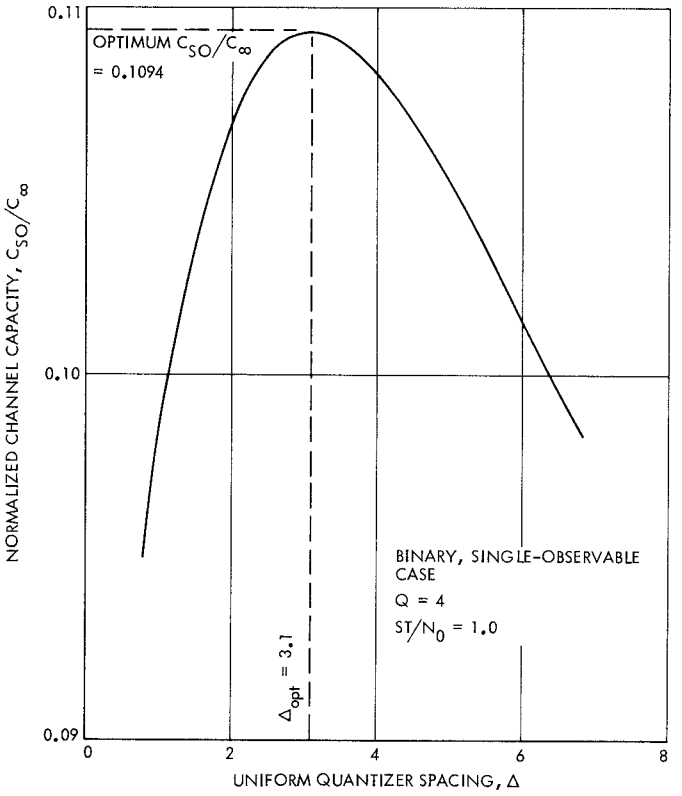

Fig. 4. Variation of capacity with quantizer spacing for binary single-observable case

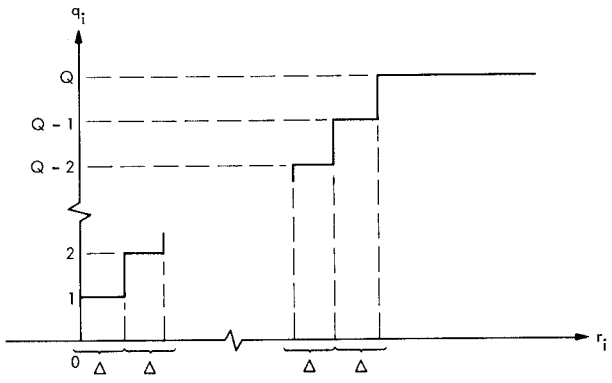

Fig. 5. Quantization rule for *i*th envelope detector output (general *M*-ary case)

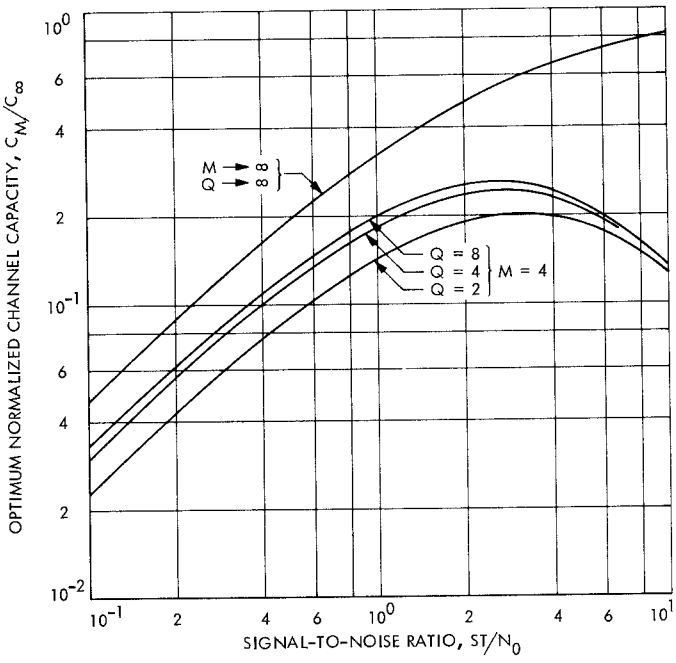

Fig. 7. Capacity for 4-ary noncoherent soft-decision MFSK system

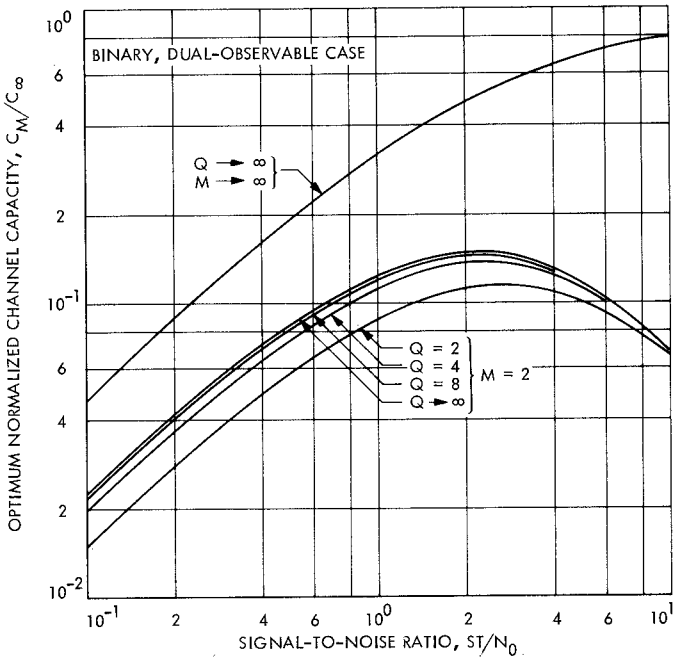

Fig. 6. Capacity for binary noncoherent FSK system based on dual uniformly quantized observables

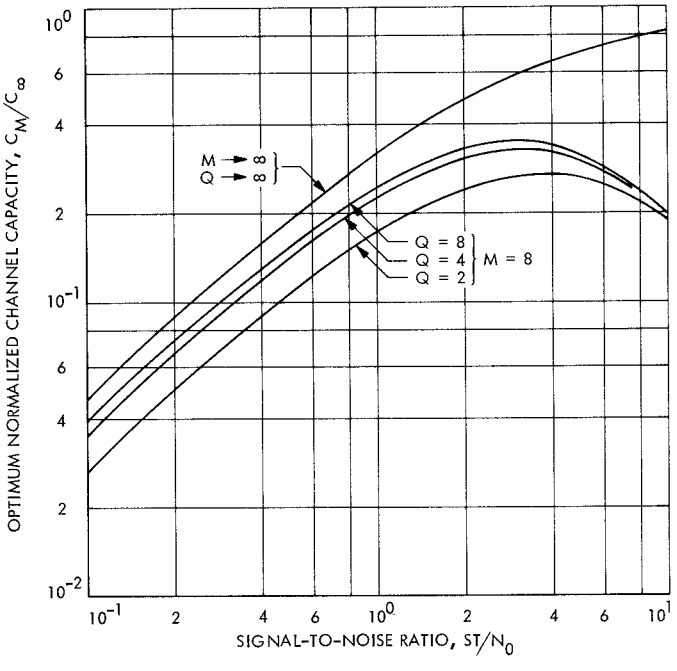

Fig. 8. Capacity for 8-ary noncoherent soft-decision MFSK system

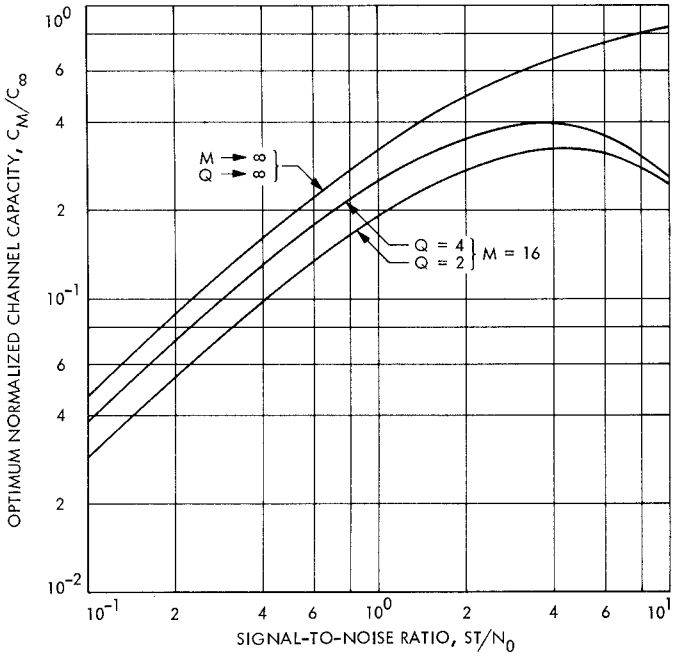

Fig. 9. Capacity for 16-ary noncoherent soft-decision MFSK system

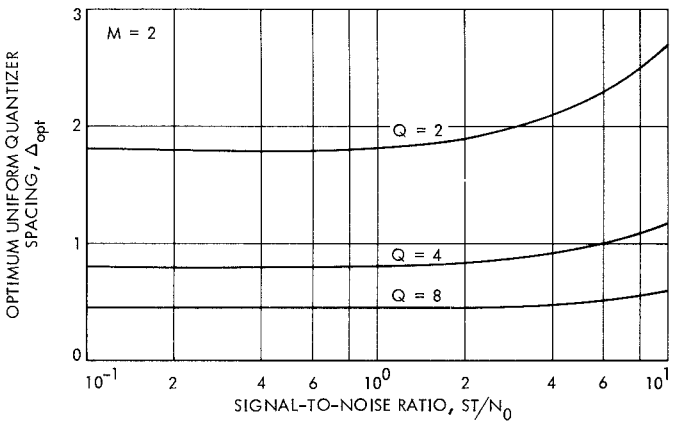

Fig. 10. Optimum quantizer spacing for binary dual-observable case.

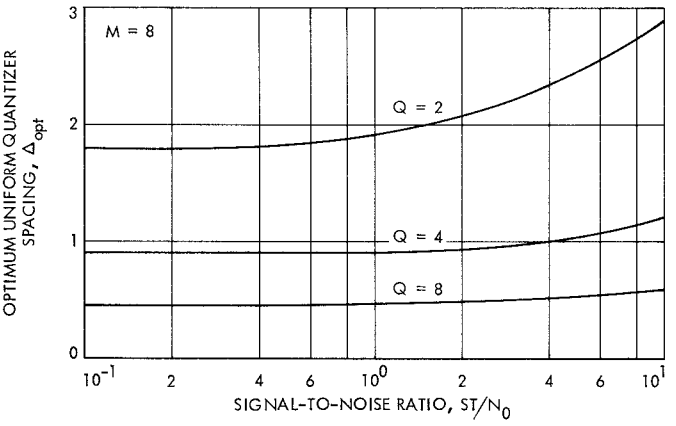

Fig. 11. Optimum quantizer spacing for $M = 8$ case

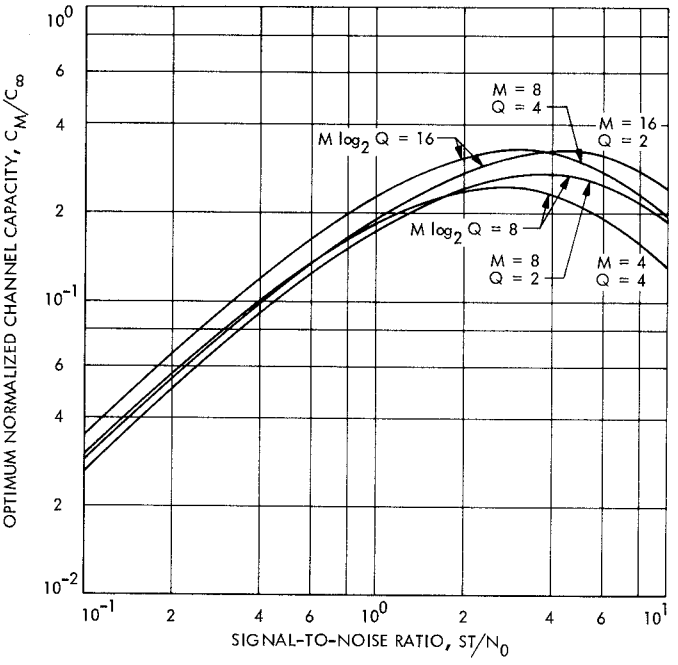

Fig. 12. Tradeoff between number of signals and number of quantization levels

Appendix
Reduction of Capacity Computation Time

The normalized capacity expression in Eq. (20) contains the factor

$$\sum_{\mathbf{q}'} f(\mathbf{q})$$

which requires the summation of Q^{M-1} terms for each q_1; the computation time therefore grows exponentially with M, for a given Q. For example, it required 100 minutes of computer time to determine C_M/C_∞ for the (8, 4) receiver at selected values of Δ and α, using Eq. (20). With the reduction technique described below, the same results were obtained with a computer execution time of only 2 minutes.

For a given q_1, many distinct vectors $\mathbf{q}'$ may yield the same argument $f(\mathbf{q})$ in the summation above. Suppose $\mathbf{q}'$ contains ℓ_1 components that are 1, ℓ_2 that are 2, $\cdots$, and ℓ_Q that are Q. Then $\mathbf{q}'$ can be (irreversibly) mapped into the vector $\boldsymbol{\ell} \equiv (\ell_1, \ell_2, \cdots, \ell_Q)$, with components in the range $0 \leq \ell_i \leq M-1$, subject to the constraint

$$\sum_{i=1}^{Q} \ell_i = M - 1$$

The significance of this mapping is that every $\mathbf{q}'$ which maps into the same equivalence class $\boldsymbol{\ell}$ produces the same term $f(\mathbf{q}) \equiv g(q_1, \boldsymbol{\ell})$, for a given q_1, where

$$g(q_1, \boldsymbol{\ell}) = \prod_{i=1}^{Q} y'^{i}(i) \ln\left[z(q_1) + \sum_{j=1}^{Q} \ell_j z(j) \right] \tag{A-1}$$

from Eq. (20). It can be seen that there are

$$n(\boldsymbol{\ell}) = \frac{(M-1)!}{\prod_{i=1}^{Q} (\ell_i!)} \tag{A-2}$$

distinct vectors $\mathbf{q}'$ which map into a particular equivalence class $\boldsymbol{\ell}$. Therefore, the summation of interest can be written in the form

$$\sum_{\mathbf{q}'} f(\mathbf{q}) = \sum_{\boldsymbol{\ell}} n(\boldsymbol{\ell})\, g(q_1, \boldsymbol{\ell}) \tag{A-3}$$

The advantage is that the original summation contained Q^{M-1} terms, while the new one has only

$$\binom{Q + M - 2}{M - 1}$$

terms.* The computational reduction factor is of the order of

$$\gamma \equiv \frac{\binom{Q + M - 2}{M - 1}}{Q^{M-1}} \tag{A-4}$$

For example, this reduction factor is tabulated below for several values of M and Q:

M	Q	γ
4	8	0.25
8	4	0.0075
8	8	0.0016

The vectors $\boldsymbol{\ell}$ can be generated recursively using a subroutine suggested by H. Rumsey. Start with the initial vector $\boldsymbol{\ell} = (M-1, 0, 0, \cdots, 0)$ and recursion parameter $p = 1$. Each successive $\boldsymbol{\ell}$ is then generated by the computer subroutine GEN $(\boldsymbol{\ell}, p)$, described by the flow chart in Fig. A-1, culminating in the final vector

$$\boldsymbol{\ell} = (0, 0, \cdots, 0, M-1)$$

Summarizing our results, the normalized capacity should be computed from the expression

$$\frac{C_M}{C_\infty} = \frac{2}{\alpha^2} \left\{ \ln M - \sum_{q_1=1}^{Q} x(q_1) \left[\sum_{\boldsymbol{\ell}} n(\boldsymbol{\ell})\, g(q_1, \boldsymbol{\ell}) - \ln z(q_1) \right] \right\} \tag{A-5}$$

in terms of previously defined parameters.

*Proved by M. Klass, Caltech Postdoctoral Fellow in Mathematics.

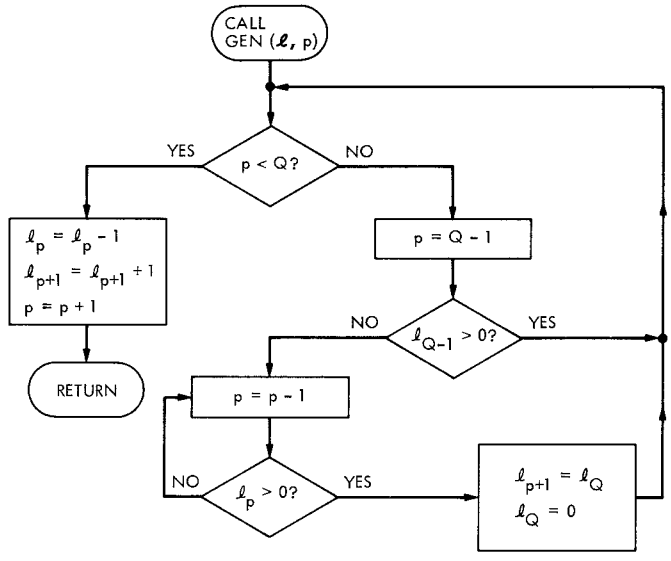

Fig. A-1. Flow chart for computer subroutine GEN (ℓ,p)